THE AMERICAN MINERALOGIST, VOL. 43, NOVEMBER–DECEMBER, 1958

ISOGYRES IN INTERFERENCE FIGURES

W. BARCLAY KAMB, *California Institute of Technology, Pasadena, Calif.**

ABSTRACT

The use of skiodromes in interpreting interference figures of crystal plates leads to both qualitative and quantitative errors, and should be abandoned. The theory of isogyre patterns is correctly developed by considering the effect on isogyre position of "rotation" of the polarization plane by the optical system. Although the amount of the rotation may be 10°–15°, its effect on isogyre position is found to be small because the effects of rotation above and below the crystal plate work in opposite directions. An analysis, based on this conclusion, of the uniaxial flash figure, acute and obtuse bisectrix figures, and optic normal figure leads to isogyre equations from which can be calculated the angle of rotation of the stage (from extinction) required to disperse the isogyres from the field. The formulas are simple and convenient, and are verified experimentally by comparison with values measured upon oriented thin sections. They provide a means of measuring $2V$ in *Bxo* figures and in *Bxa* figures of large $2V$, and in particular a means of distinguishing between *Bxa* and *Bxo* figures. The corresponding formulas given by the skiodrome theory and the theory of Michel-Lévy are not satisfactory. An analysis of the optic axis figure reveals that 45° isogyre curves derived by Wright upon seemingly unsound assumptions are in fact surprisingly accurate. Replacements for the skiodromes currently in use are mentioned.

1. Introduction

The theory of interference figures in crystal optics was developed mainly between about 1900 and 1925. Most of the results and methods of this early work have fallen into disuse. In explaining the origin and form of isogyres, recent textbooks (Wahlstrom, 1951; Burri, 1950) make use exclusively of the skiodrome, a device introduced originally by Becke (1904). The skiodrome is, however, an incorrect representation of interference phenomena. It is physically unsatisfactory, and leads to incorrect predictions as to the positions and shapes of isogyres.

With the hope of correcting this situation, the present paper advances a coherent theory of the positions of isogyres in interference figures. The theory is subjected to practical test with the petrographic microscope, and its predictions are compared directly with the predictions of the skiodrome theory and other representations of interference phenomena. As a result of these tests (aside from the reasoning behind the theory) one may conclude that the theory here developed accounts correctly for the positions of isogyres, and that the older theories do not. On the basis of the theory a practical means for distinguishing between *Bxa* and *Bxo* figures can be established, and a method given for measuring $2V$ in figures of either kind.

* Division of Geological Sciences, contribution No. 865.

2. History of isogyre theory

A survey of the literature on the isogyre problem reveals three main lines of development: (1) a protracted dispute (1904–1923) between F. Becke and F. E. Wright over the proper method of measuring $2V$ from interference figures; (2) introduction of the skiodrome theory by Becke, and its subsequent interpretation and development by Johannsen, and others; (3) formulation and application of approximate isogyre equations by Michel-Lévy and Wright.

The dispute between Becke and Wright arose from the following question. Suppose that at a given point in the interference field of the conoscope, the direction of vibration (direction of electric displacement $\boldsymbol{D}$) of light reaching the observer's eye is known. What is the direction of $\boldsymbol{D}$ of the corresponding ray of light while traversing the crystal plate under observation? Becke and Wright proposed different constructions (in stereographic projection) for the solution of this problem, and in the years 1904–1925 disputed the correctness of one another's methods (Becke, 1904; Wright 1907; Becke, 1909; Wright, 1911; Kaemerer, 1913; Souza-Brandao, 1914; Wright, 1923). A review of the course of the dispute can be found in Wright's 1923 paper (pp. 807–809). In this paper Wright concluded that the correct construction is unknown, and that there is in general an uncertainty equal roughly to the difference between the Becke and Wright methods in translating the position of isogyres in an interference figure into conditions in the crystal plate that produce the figure. The interpretation of interference figures is, he concluded, inherently approximate at best.

This conclusion was probably responsible for the lack of further development of the theory of interference figures. Discrediting the older "exact" methods of analyzing interference figures, it was probably responsible for the abandonment of these methods and the reliance instead exclusively on the skiodrome theory, a theory developed along lines quite different from those of the "exact" methods, but one which led to convenient diagrams and easily visualized conclusions.

The skiodrome actually had been introduced by Becke in 1904. Whether it was intended as an exact theory or simply a handy tool is difficult to judge from the original article, but in the hands of others it was treated as an exact theory and developed in considerable detail to give isogyre equations for various types of interference figure. A detailed development of the skiodrome theory can be found in Johannsen's textbook (1918, pp. 429–440).

Nowadays the skiodrome theory seems to be used mainly as a device for demonstrating qualitatively to students the origin and general pattern of isogryes. The exact numerical development of the theory seems largely to

be disregarded. Neverthless, the emphasis placed on the skiodrome theory suggests that it should provide a more accurate description of isogyres if such a description were needed.

An accurate description was, in fact, required by Michel-Lévy in an early work (1888) in which he proposed a method for determining $2V$ from bisectrix figures. For this purpose he developed an equation for the isogyres in bisectrix figures, by treating the interference phenomena as though they took place in a plane and applying the planar analog of the law of Biot and Fresnel. Wright (1905) rederived his formula but pointed out (1907, p. 341) that it did not seem to give trustworthy results and recommended that it not be used. Nevertheless, he applied the same type of analysis to the optic axis figure, obtaining an equation for the isogyre in the 45° position, from which he calculated the isogyre curves that have been reproduced in almost every optical mineralogy textbook.

Present day teaching and practice in interference figure interpretation are outgrowths of these three unrelated lines of approach to the isogyre problem. In this paper I want to show that the skiodrome theory is patently incorrect and should be discarded. A theory to replace it can be formulated when it is shown that the dispute between Becke and Wright failed to recognize the factors that actually determine the position of isogyres. The application of the new theory to bisectrix and flash figures provides a test of the theory against the predictions of the skiodrome theory and the theory of Michel-Lévy. Finally, the new theory can be applied to the optic axis figure and the result compared, for the 45° position, with the equation and curves given by Wright (1905).

3. The skiodrome theory

The skiodrome theory consists of two distinct elements: (1) definition and details of construction of the skiodrome corresponding to a given interference figure; (2) interpretation of the skiodrome in terms of the positions and shapes of isogyres, and justification of this interpretation.

A skiodrome of a given crystal plate is an orthographic projection of curves of constant wave index of refraction ("isotaques") plotted on the surface of a sphere, which may be called the "reference sphere" for the crystal under consideration.* The details of this construction are given in most textbooks.

Interpretation of the skiodrome is based on an analogy with the phenomenon of extinction in orthoscopic light: the isogyres are said to be located

* Evans (1907), who first introduced the theory into the English language, called the individual projected isotaques "skiodroms." Nowadays the term "skiodrome" is used confusingly both for the individual curves, and for the entire figures which they compose. I shall use the term only for the entire figure.

at those points in the interference field where the allowed directions of $\boldsymbol{D}$ in the crystal coincide with the directions transmitted by the polarizer or analyzer. If one were to start from this assumption, he would need to determine what direction of $\boldsymbol{D}$ in the crystal plate corresponds to an observed direction of $\boldsymbol{D}$ at a given point in the interference field. This is exactly the question disputed by Becke and Wright. Becke's and Wright's methods of determining $2V$ from the isogyre patterns are based, in fact, on the above assumption and on the separate constructions which the two men proposed as the solution of the resulting problem.

The skiodrome theory, however, presents an entirely different solution to the problem, because it asserts in effect that the allowed directions of $\boldsymbol{D}$, as seen in the interference field, correspond to the tangents (and normals?) to the projected equirefringence curves in the skiodrome. This construction leads to predicted directions of $\boldsymbol{D}$ that differ by as much as 90° from the directions given by the Becke or Wright constructions.

It is difficult to see why Becke, who proposed the skiodrome approach to the isogyre problem, should have thereby chosen a method which gives predictions so greatly different from his own "exact" solution of the $\boldsymbol{D}$-direction construction. The only justification for the skiodrome method, as far as I can see, is that the interference phenomena do take place in effect on the focal sphere of the hemispherical objective lens, and this focal sphere, when observed from the distance of the ocular, is for practical purposes projected onto a plane perpendicular to the microscope axis—a fact that is responsible for the validity of Mallard's law. The fact that the focal sphere is observed in orthographic projection does not necessarily mean that the directions of $\boldsymbol{D}$ on the focal sphere are orthographically projected when viewed from the ocular, and I shall in fact show that this is definitely not the case.

Consider the allowed directions $\boldsymbol{D}_1$ and $\boldsymbol{D}_2$ corresponding to a given wave normal direction $\boldsymbol{n}$ in a crystal, shown in stereographic projection in Fig. 1. The pole of the projection is the microscope axis. When the waves 1 and 2, having wave normal $\boldsymbol{n}$ in the crystal, have been refracted by the objective lens so as to travel up the microscope tube their directions of $\boldsymbol{D}$ are now $\boldsymbol{D}_1'$ and $\boldsymbol{D}_2'$, if determined from the Becke construction, or $\boldsymbol{D}_1''$ and $\boldsymbol{D}_2''$, if determined from the Wright construction. In the Becke construction, the directions are rotated about the horizontal axis N until they are horizontal, N being the intersection of plane $\boldsymbol{D}_1\boldsymbol{D}_2$ (which is normal to $\boldsymbol{n}$) with the horizontal plane. (By "horizontal" is meant "parallel to the microscope stage.") Thus $\boldsymbol{D}_1'$ and $\boldsymbol{D}_2'$ lie on the small circles, drawn about N as center, that pass through $\boldsymbol{D}_1$ and $\boldsymbol{D}_2$. In the Wright construction, the "vibration planes" $\boldsymbol{D}_1\boldsymbol{n}$ and $\boldsymbol{D}_2\boldsymbol{n}$ are intersected with the horizontal plane to find the final directions of $\boldsymbol{D}$. Thus

D_1'' and D_2'' lie at the ends of the great circles passing respectively through D_1 and n and through D_2 and n.

The skiodrome construction gives final directions D_1''' and D_2'''. These are derived by orthographic projection of the vectors D_1 and D_2. Since azimuthal directions are the same in orthographic or stereographic projection of a sphere, D_1''' and D_2''' evidently lie at the ends of radii from the pole of the projection, passing respectively through D_1 and D_2.

The geometry of small circles and great circles in stereographic projection requires that D_1' and D_1'' always lie on the same side of D_1''', except

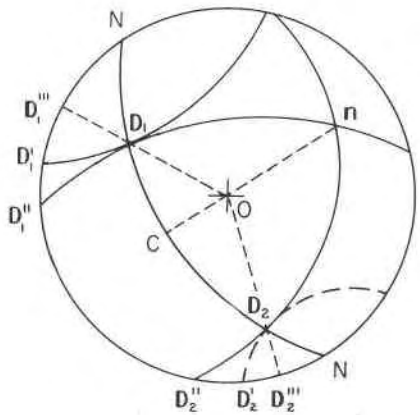

FIG. 1. Stereographic projection to illustrate the Becke, Wright, and Skiodrome constructions for finding the D vector in the interference field from the D vector in the crystal. n is a wave normal in the crystal, and D_1, D_2, the associated directions allowed for D. o is the microscope axis.

in the case that D_1 lies at C or N, in which event the three points D_1', D_1'', and D_1''' coincide. This fact can be justified in detail but is obvious without detailed proof. Hence the skiodrome point D_1''' always lies *outside* the range of directions between D_1' and D_1'', and a similar statement applies to D_2'''. The one certain conclusion from the Becke-Wright controversy is, however, that a correct construction would place the final direction of D between D_1' and D_1'', and between D_2' and D_2''. Thus the skiodrome construction cannot possibly give the correct D directions except for points on the reference sphere where D is either horizontal, or lies in a vertical plane containing n. For all other points the skiodrome construction is wrong.

This objection is fundamental, but another objection can be raised independently. For all except the centered uniaxial optic axis skiodrome, and at all points on the skiodromes except the center and in some cases

points on the edge, the orthographically projected equirefringence curves are not orthogonal, so that the allowed ***D*** directions given by the skiodrome are not perpendicular when they reach the interference field of the microscope. The skiodrome theory takes account of this circumstance in a clever but puzzling way. It asserts that there are, in fact, always two isogyres, one in which the projected meridianal equirefringence curves are parallel to the directions of ***D*** transmitted either by the polarizer or the analyzer (which we will henceforth regard as NS and EW respectively), called the meridianal isogyre, and one in which the projected equatorial curves are parallel to NS or EW, called the equatorial isogyre. The two isogyres are superposed to form the isogyre actually observed, and since a doubling, even faintly, of the isogyre is never observed, the theory supposes that the two isogyres are broad and overlap to such an extent that the actual isogyre appears simply as a "broad brush" where the two separate significantly, an interpretation that correlates qualitatively with the observed features of isogyres.

Even if a qualitative explanation were adequate for all purposes, the skiodrome theory would have to be discarded, because its predictions are qualitatively wrong for at least one type of figure, the biaxial optic normal figure. The skiodrome for this case predicts that the meridianal and equatorial isogyres should lie in adjacent quadrants of the interference field. As the crystal plate is rotated away from the extinction position, in which the isogyres form a centered cross, the cross should break up into four hyperbolic isogyres which move out into the four quadrants of the field. The meridianal isogyres move into the quadrants into which the acute bisectrix also moves, and the equatorial isogyres move into the other two quadrants. The equatorial isogyres disappear from the field more rapidly than the meridianal isogyres. For $2V = 90°$ the stage must still be rotated about 4° before the isogyres (which in this case move out equally fast in all four quadrants) reach the edge of the field.

One need only examine an appropriate thin section, however, to see that the optic normal cross breaks up into only two isogyres, and these move into the quadrants into which the acute bisectrix moves. As $2V$ approaches 90°, the figure becomes less and less distinct, and the isogyres leave more and more rapidly, until for $2V = 90°$ the dark field simply vanishes as the stage is rotated from the extinction position, without breaking up clearly into hyperbolic curves at all.

If the skiodrome theory fails qualitatively, its quantitative applications can hardly be of much value. One example had already been given—the angle of rotation of the crystal plate required to bring the optic normal isogyres for $2V = 90°$ to the edge of the interference field. For a conoscope of numerical aperture 0.85 the calculated angle is about 4°, which is

actually close to the observed angle for the isogyres in a uniaxial flash figure. Thus, if the skiodrome theory were correct, optic normal figures for which $2V=90°$ would resemble uniaxial flash figures quite closely, except that there would be four isogyres instead of two.

In most cases it is difficult to propose a quantitative test of the skiodrome theory, because the theory provides no method by which the two types of isogyre should be combined to get the actual isogyre. Such a method cannot be found, because the theory has no physical meaning which would enable one to calculate the amount of light transmitted by the analyzer for a given point in the interference field with a given configuration of projected equirefringence curves. In short, a theory that defies the laws of optics is difficult to interpret quantitatively.

Nevertheless, there is one interference figure that provides a quantitative test of the skiodrome theory, the uniaxial flash figure. The skiodrome for this case shows that there will be no equatorial isogyres, but instead a uniform change in illumination of the field as the crystal plate is rotated. Thus the isogyres in the uniaxial flash figure must be solely the meridianal ones of the skiodrome theory, for which a definite position can be calculated. The calculation (section 6) shows that the predicted isogyres leave the field exactly half as rapidly as actually observed. This is a decisive test and shows definitely that the skiodrome theory is wrong, even when applied only to the inner portion of the interference field.

4. The effect of "rotation," and the "isotropic cross"

Because the effects that produce the "isotropic cross" are important in determining the location of isogyres, it is necessary to discuss them.

Whenever a light wave passes through a refracting surface, a certain fraction of the energy is transmitted and a certain fraction reflected. If the light wave is plane polarized with $\boldsymbol{D}$ in the plane of incidence, a greater fraction of the incident energy is transmitted than if the wave is polarized with $\boldsymbol{D}$ perpendicular to the plane of incidence (i.e., $\boldsymbol{D}$ parallel to the refracting surface).

A plane polarized light wave with $\boldsymbol{D}$ intermediate in orientation between the incident plane and its normal will therefore suffer a greater diminution of the component perpendicular to the incident plane than of the component parallel to the incident plane, in passing through the refracting surface. This relative decrease in the perpendicular component of the $\boldsymbol{D}$ vector is responsible for a "rotation" of the vector away from the orientation that would be calculated by Becke's method.

The amount of this rotation can be calculated from the electromagnetic theory. A different derivation was given by Wright (1923, pp. 796–797), but his method lacks a physical basis. Moreover, there are misstatements

and misprints in the derivation and his final result is wrong; it is valid for a wave travelling in the direction opposite to the one assumed in the derivation.

Suppose that the $\boldsymbol{D}$ vector amplitude of the incident plane polarized wave, moving in a medium of index n_i, has components $D_i^{\parallel}$ in the incident plane and component $D_i^{\perp}$ perpendicular thereto. The incident wave normal $\boldsymbol{n}_i$ makes an angle θ_i with the normal to the refacting surface. $\boldsymbol{D}_i$ is of course perpendicular to $\boldsymbol{n}_i$. The refracted wave, in medium of index n_t, then has components

$$D_t^{\parallel} = D_i^{\parallel} \frac{2n_t \cos\theta_i}{\sqrt{n_t^2 - n_i^2 \sin^2\theta_i} + \frac{n_t^2}{n_i}\cos\theta_i}$$

$$D_t^{\perp} = D_i^{\perp} \frac{2n_i \cos\theta_i}{\sqrt{n_t^2 - n_i^2 \sin^2\theta_i} + n_i \cos\theta_i}.$$

The derivation of these results can be found in works on electromagnetic theory. From these equations, and with the help of Snell's law,

$$n_i \sin\theta_i = n_t \sin\theta_t$$

the value of the ratio $D_t^{\perp}/D_t^{\parallel}$ is found (after some manipulation) to be simply

$$\frac{D_t^{\perp}}{D_{t\parallel}} = \frac{D_i^{\perp}}{D_{t\parallel}} \cos(\theta_i - \theta_t). \tag{1}$$

The decrease in the ratio $D^{\perp}/D^{\parallel}$ is thus independent of the sign of $\theta_i - \theta_t$. The situation is depicted in stereographic projection in Fig. 2. In terms of the angles ν_i and ν_t, (1) can be written

$$\tan\nu_t = \cos(\theta_i - \theta_t)\tan\nu_i, \tag{2}$$

a formula first obtained by Fresnel.

It can be shown that (2) leads to the conclusion that $\boldsymbol{D}_i$ and $\boldsymbol{D}_t$ lie on a great circle through $\boldsymbol{n}_i$, as shown in Fig. 2. This conclusion is the basis for Wright's construction, mentioned previously.

Note that if it were true that $\nu_t = \nu_i$, then $\boldsymbol{D}_i$ and $\boldsymbol{D}_t$ would lie on a small circle centered at N, the normal to the incident plane. This is Becke's construction. Actually $\nu_t < \nu_i$, so that the $\boldsymbol{D}$ vector is "rotated" toward the incident plane by the amount $\delta = \nu_i - \nu_t$.

In an interference figure, the only light that reaches the observer's eye is light that has travelled almost straight up the microscope axis from each point on the interference sphere (focal sphere of the objective lens). Thus, the only light that is seen from a given point P on the interference sphere is light that has been refracted through the optical system in a plane of incidence always containing the microscope axis and P.

At the corresponding point P in the interference figure (Fig. 3), the

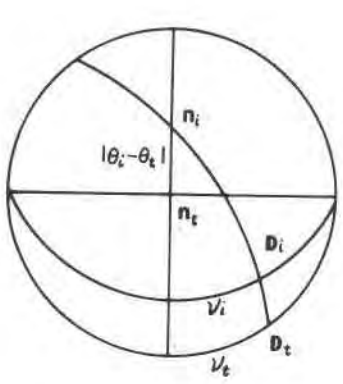

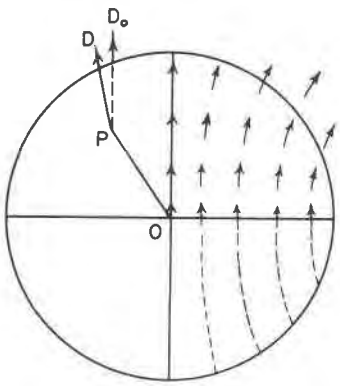

FIG. 2 (left). Stereographic projection to illustrate the "rotation" of the ***D*** vector caused by refraction of plane polarized light. n_i is the incident wave normal, which is refracted to n_t. D_i and D_t are the corresponding directions of ***D***. The orientation of the refracting surface is not plotted.

FIG. 3 (right). Pattern of ***D***-vectors in the interference field of the conoscope. The pattern, shown in the NE quadrant, can be extended symmetrically to the rest of the field, as suggested.

light would have ***D***-direction PD_o if ν_t were equal to ν_i at every refraction in the lens system. But in fact the component of PD_o perpendicular to OP is reduced relative to the component parallel to OP, so that the actual direction of ***D*** at P is rotated toward OP (prolonged), to some orientation such as PD. The resulting directions of ***D*** in the interference field form the pattern shown in the NE quadrant of Fig. 3, in which it is assumed that the polarizer is set to transmit ***D*** accurately NS. Such a pattern was described by Wright (1923).

The pattern shown in Fig. 3 is responsible for the isotropic cross, and can be verified by rotating the polarizer (or analyzer) of the microscope. The cross breaks up into two hyperbolic curves. If the ***D*** direction transmitted by the polarizer, which will be called the polarization direction, is rotated into the NW–SE quadrants of the field, the hyperbolae move into the NE and SW quadrants, and vice versa. By rotating the polarizer, the amount of "rotation" δ at any point in the field can be measured. The maximum value for the lens system alone (without any plate inserted between the condenser and objective) is about 6° or 7° for most microscope lens combinations of half-aperture close to 60° (in air).

The isotropic cross described above is produced without birefringence or path differences, as can be tested with the gypsum plate. Johannsen (1918, p. 416), however, refers to the cross as having "weakly uniaxial positive character." In this statement he confuses the above isotropic cross with a second "cross" that can be observed when the microscope is

adjusted improperly. The first cross, described above, is observed when the cone of light coming directly from the light source, converged by the condensing system, fills the field of the conoscope, so that the image of the light source, seen in the interference field, fills the entire field. If the microscope tube is then raised, the image of the light source shrinks rapidly. Superposed upon the image of the upper face of the condenser, which does not shrink so rapidly, can be seen a second "cross." It can better be observed by substituting a small bright light source for the usual diffuse one—for example, by removing the blue diffusing plate used in most lamps. A gypsum plate shows that path differences are associated with this cross (in some microscopes). If the cross were interpreted as uniaxial, its sign would be +, as noted by Johannsen. When the polarizer is rotated, the cross of the second kind behaves very differently from the cross of the first kind, as shown in Fig. 4 (row II).

Upon raising the microscope tube further, so that the image of the condenser face shrinks down into the center of the field, a third kind of cross can be observed in the remainder of the field. It can also be seen simply by swinging the movable substage condenser out of the optical train. It has no "uniaxial" character. Upon rotating the polarizer the cross breaks up into a pair of hyperbolae that move slowly out into the same quadrants as the direction of polarization does, as shown in Fig. 4, row III.

The crosses of the second and third kinds are produced by light that has been twice or more *reflected* at lens surfaces in the optical train. If a beam of perfectly parallel light enters the condensing system from below, the light reflected by the lens surfaces from rays that do not travel exactly along the condenser axis forms, after a second reflection that sends the light in a general upward direction again, a broad weak cone of light diverging at all angles from the main light cone. The light in this cone is polarized with $\boldsymbol{D}$ nearly perpendicular to the plane of incidence, because the perpendicular component is preferentially reflected. That portion of the twice reflected light that has been reflected at the polarizing angle will have $\boldsymbol{D}$ exactly perpendicular to the incident plane. The twice (or more) reflected light from the condenser forms the cross of the second kind, and light similarly reflected in the objective forms the cross of the third kind.

A plot of the expected direction of $\boldsymbol{D}$ after *one* reflection is shown in Fig. 5. The plot is qualitative only. Radial distance is angle of incidence plotted stereographically. The solid circle is drawn at the polarizing angle. The polarizer is set NS. To determine the directions of $\boldsymbol{D}$ expected in the multiple reflected light from the actual lens combinations requires a knowledge of the paths of the reflected rays, and hence a detailed knowledge of the lens system design. However, it can be shown rather simply

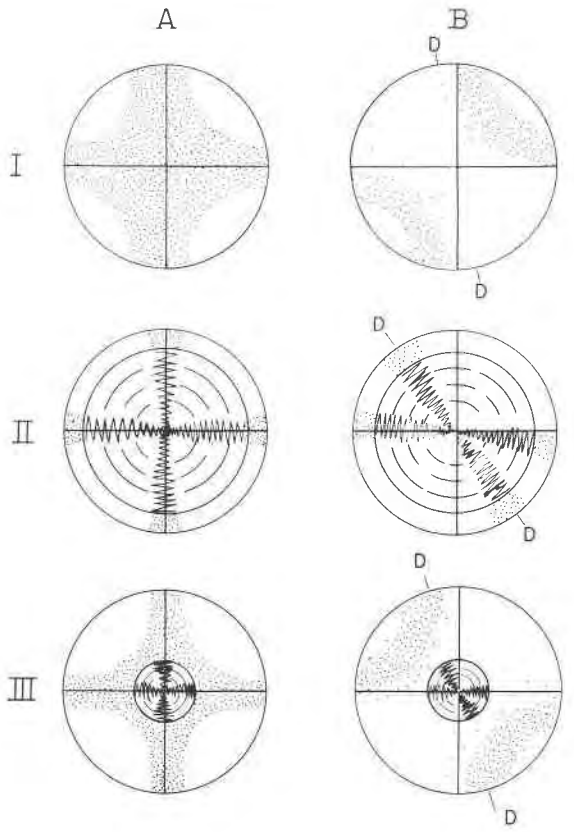

FIG. 4. The three types of "isotropic cross" seen in the conoscope field. Column A shows the centered cross seen when the polarizer is set NS and the analyzer EW. When the polarizer is turned to the position DD, the cross breaks up into the form shown in column B. The circular object within the field in rows II and III is the image of the upper face of the substage condenser.

that the twice reflected light from the objective which appears at a given point in the interference field can have been reflected at an angle of incidence at most equal to the angle, in glass, corresponding to the distance of the given point from the center of the field. At the edge of the field this angle is about 30°, much less than the polarizing angle (56° for $n=1.50$), so that a distribution of vectors roughly similar to that shown inside the solid circle in Fig. 5 may be expected for the cross of the third kind. This conclusion is in agreement with the behavior of the cross upon rotation of the polarizer. Thus, if the analyzer transmits in the direction AA in Fig. 5, a dark curve would be expected to follow the heavy dotted line shown.

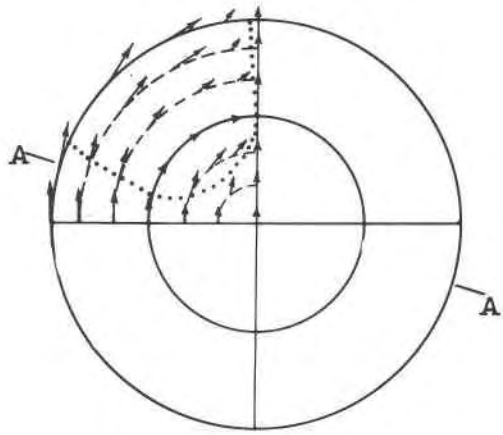

FIG. 5. Direction of $\boldsymbol{D}$ after one reflection of plane polarized light. The directions are shown as short arrows stereographically projected into the plane of the drawing from their actual position in space. The incident light is polarized in such a way that before reflection all the arrows would have been NS. Radial distance is angle of incidence plotted stereographically. The diagram is qualitative only. The solid inner circle corresponds to the polarizing angle.

The cross of the second kind behaves in a way appropriate to the outer portion of Fig. 5. I do not know the exact reason for this, but it appears that the light must have been reflected several times.*

A more exact analysis of the crosses of the second and third kinds would be interesting, but it is unnecessary for a discussion of interference figures, which are observed in the strong direct beam of light from the light source, to which the discussion leading to Fig. 3 applies. It is reasonable to assume that the weak light responsible for the crosses of the second and third kinds, which are always superposed on the interference field of the direct light, will have a negligible effect on the appearance of the interference figure. This is evident in observing the behavior of the isotropic cross of the first kind, which blots out the other two crosses.

5. Location of the isogyres

The isogyres are regions in the interference figure where the light inten-

* The path differences exhibited by the cross of the second kind are doubtless due to strain birefringence caused by internal stresses in the lenses of the substage condenser. In all internally stressed lenses that I have examined, the birefringence has radially-slow character, as observed in the cross of the second kind. All Leitz microscopes that I have examined show the presence of these internal stresses. The new Zeiss research and student models, however, have stress-free substage condensers, and the cross of the second kind in these microscopes shows no path differences.

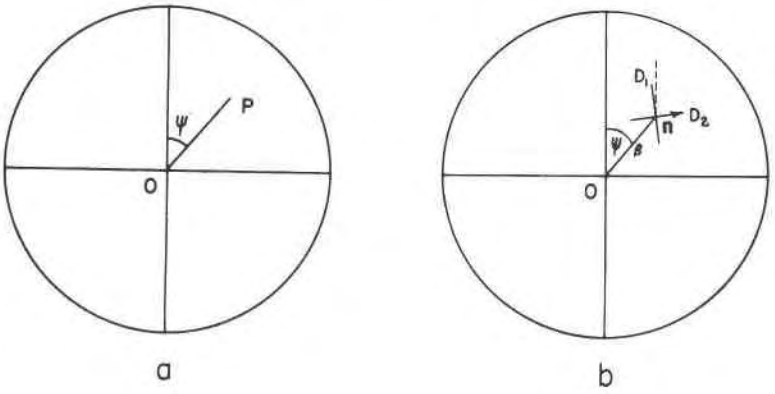

FIG. 6. Diagrams to illustrate the factors that determine isogyre position. 6*a*, orthographic projection; 6*b*, stereographic projection.

sity transmitted by the analyzer is locally a minimum. We therefore ask, for a given point P in the interference field (Fig. 6*a*), what orientation of the allowed directions of $\boldsymbol{D}$ for the corresponding wave normal in the crystal will minimize the light intensity from P transmitted by the analyzer? The allowed directions are shown as a small cross in the stereographic projection of Fig. 6*b*. Note that a stereographic projection of the cross is equivalent to rotating the cross from the reference sphere into the horizontal plane by Becke's construction, that is, about a horizontal axis perpendicular to OP at P.

Figures 7*a* and 7*b* are magnifications of a small region about $\boldsymbol{n}$ and P in Fig. 6*b* and 6*a*. The vector $\boldsymbol{D}$ of the plane polarized light wave that enters the base of the crystal plate is resolved into two components $\boldsymbol{D}_1$ and $\boldsymbol{D}_2$. The birefringence is assumed small enough that $\boldsymbol{D}_1$ and $\boldsymbol{D}_2$ can be considered to lie in the same plane, so that $\boldsymbol{D}_1$ and $\boldsymbol{D}_2$ are perpendicular. The dashed axes lie NS and EW. If there were no "rotation" of the $\boldsymbol{D}$ vector in passing from the polarizer to the crystal plate via the condensing system, $\boldsymbol{D}$ would lie along NS. Instead, it has been rotated an amount δ_1 toward On. ξ defines the orientation of the allowed directions of $\boldsymbol{D}$. At the top of the crystal plate the resolved waves 1 and 2 can be written

$$\begin{aligned} D_1' &= D\cos(\xi + \delta_1)e^{-i\omega t} \\ D_2' &= D\sin(\xi + \delta_1)e^{-i\Phi - i\omega t} \end{aligned} \tag{3}$$

where a phase shift Φ between the two waves is produced in traversing the crystal plate.

Next the effect of rotation in the remainder of the optical system must be accounted for. We suppose that ξ is small enough that the rotations of the plane polarized waves D_1' and D_2' are the same as for waves with

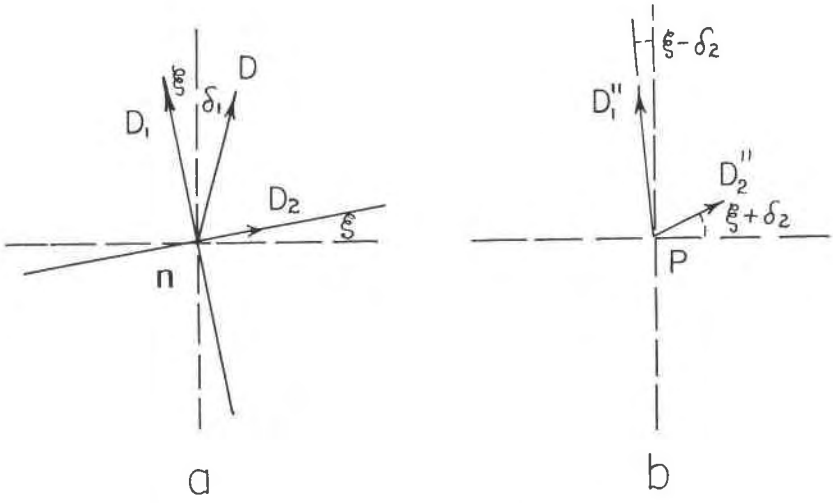

FIG. 7. Enlargements of portions of Fig. 6. 7*a* represents the region around ***n*** in Fig. 6*b*. 7*b* shows the ***D*** vectors in the light that reaches the analyzer from the point *P* in Fig. 6*a*.

$\xi = 0$. The condition for this is $\xi \ll \psi$, which we will verify *a posteriori* to be satisfied, because when $\psi \sim 45°$, $\xi \sim 1°$ at most. It will develop later that the amount of rotation for D_1 varies as $\sin 2\psi$, and is therefore equal for ψ and $\pi/2 - \psi$, so that D_1' and D_2' are rotated by equal amounts δ_2, both toward the incident plane On, as shown in Fig. 7b. It can be shown that if δ_2 is small the two waves are attenuated by nearly the same factor C owing to the energy carried away by the reflected light, so that we can write for the amplitudes D_1'' and D_2'' of the waves that arrive at the analyzer:

$$D_1'' = C\kappa_1 D_1', \qquad D_2'' = C\kappa_2 D_2' \tag{4}$$

where C is a constant factor independent of ξ, κ_1 and κ_2 are functions of ψ and δ_2 and can be shown to be

$$\kappa_1 = 1 - \delta_2 \tan\psi + \cdots, \qquad \kappa_2 = 1 - \delta_2 \cot\psi + \cdots$$

to the first order in δ_2. Note that $\kappa_1 = \kappa_2$ for $\psi = \pi/4$. The first order terms $\delta_2 \tan\psi$ and $\delta_2 \cot\psi$ remain small for any value of ψ, because of (10), below.

The amplitude of the wave transmitted by the analyzer (set EW) is

$$D_A = -D_1'' \sin(\xi - \delta_2) + D_2'' \cos(\xi + \delta_2). \tag{5}$$

The intensity I of the light seen at P is obtained by combining (3), (4), and (5):

$$\frac{I}{C^2 I_o} = \frac{|D_A|^2}{C^2 |D|^2} = \kappa_2^2 \sin^2(\xi + \delta_1)\cos^2(\xi + \delta_2) + \kappa_1^2 \cos^2(\xi + \delta_1)\sin^2(\xi - \delta_2)$$
$$- 2\kappa_1\kappa_2 \sin(\xi + \delta_1)\cos(\xi + \delta_1)\sin(\xi - \delta_2)\cos(\xi + \delta_2)\cos\Phi \tag{6}$$

where I_o is the intensity of light entering the crystal plate at the bottom.

In keeping with the assumption that ξ, δ_1 and δ_2 are small angles (all less than about 5° in the field of the conoscope), (6) may be expanded to lowest order in powers of these quantities to obtain

$$\frac{I}{C^2 I_o} = 2\xi^2 + \delta_1^2 + \delta_2^2 + 2\xi(\delta_1 - \delta_2) - 2[\xi^2 + \delta_1\delta_2 + \xi(\delta_1 - \delta_2)] \cos \Phi. \tag{7}$$

To find the condition that P lie on an isogyre, we minimize (7) with respect to ξ:

$$[2\xi + (\delta_1 - \delta_2)](1 - \cos \Phi) = 0. \tag{8}$$

Φ applies, of course, to a given wavelength of light. Cos Φ is equal to 1 only for certain select wavelengths, so that the term $1 - \cos \Phi$ does not in general vanish for white light (for monochromatic light it locates the dark fringes). Thus the isogyre passes through points in the interference field where

$$\xi = \tfrac{1}{2}(\delta_2 - \delta_1). \tag{9}$$

This shows that the effects of rotation in the condenser and objective tend to cancel in determining the position of the isogyre. The protagonists in the Becke-Wright controversy had assumed in effect that $\xi = \delta_2$, evidently a serious error if δ_1 and δ_2 are of roughly the same size. The "correct" construction envisaged by Wright (1923) would have required ξ to be about 6° (about one half δ_{l+p} in Table 1), whereas, as we shall see below, ξ is almost certainly less than 1° in practice.

Note that the condition (9) for location of the isogyre is based on two important assumptions: (1) the birefringence of the crystal plate is small; (2) the variation of C with position in the interference field is not large enough to be significant.

To assess the size of ξ, consider first the application of (2) to the rotation produced in the microscope. If the angles of rotation are small, $\nu \cong \psi$, so that we may write for the rotation δ produced in one reflection

$$\tan (\psi - \delta) = \cos \Delta\theta \tan \psi$$

which when expanded for δ small gives

$$\delta = \sin 2\psi \sin^2 \frac{\Delta\theta}{2}. \tag{10}$$

TABLE 1

Series	I	II	III	Average
δ_{l+p}	11.4°	12.5°	11.1°	11.7°
δ_l	6.1	7.5	7.1	6.9
δ_p	5.3	5.0	4.0	4.8

For the complete rotation in the microscope

$$\delta_1 + \delta_2 = \sin 2\psi \sum_i \sin^2 \frac{\Delta\theta_i}{2} \tag{11}$$

where $\Delta\theta_i$ is the change of direction of the ray at the i'th refracting surface.

The applicability of (10) can be tested in the following way. A clean glass slide of known index of refraction is placed on the stage, and the angle of rotation for light in the interference field is measured by rotating the polarizer. In view of (10), the maximum rotation, δ max, occurs at $\psi = 45°$. δ max. is easily measured, because it requires setting the polarizer so that the center of the dark hyperbolic shadow in Fig. 4 (IB) is just tangent to the edge of the interference field. Call the rotation measured in this way δ_{l+p}. The glass slide is then removed and the rotation δ_l due to the lens system alone is measured. The difference $\delta_{l+p} - \delta_l$ is the rotation produced by the plate. Since there are two refractions of amount $\Delta\theta$ in passing through the plate, and since the rotation is measured at $\psi = 45°$, (10) predicts

$$\delta_{l+p} - \delta_l = \delta_p = 2 \sin^2 \frac{\Delta\theta}{2} \tag{12}$$

where

$$\Delta\theta = \left| \theta_i - \theta_r \right| = \theta_m - \sin^{-1} \frac{\sin \theta_m}{n} . \tag{13}$$

θ_m is the half-aperture (in air) of the conoscope, and is a constant for a given objective lens; n is the index of the glass plate.

The results of three series of measurements are shown in Table 1. The objective used is a Leitz achromatic, No. 7 (N.A. 0.85). The glass plate has $n = 1.516$, measured by the immersion method. Each measured δ value given in the table is the average of four or five individual measurements. The scatter of the results indicates the inaccuracy of such measurements. The inaccuracy arises from the diffuseness of the hyperbolic shadow. There seems also to be a personal bias in judging when the center of the shadow is set at the edge of the field, and this bias varies unpredictably from one series of measurements to another. Nevertheless, there is a general consistency in the results, and the average, $\delta_p = 4.8°$, agrees exactly with the value calculated from (12) and (13) with the assumption $\theta_m = 57.6°$, which is the value derived from isogyre measurements (section 7), for the particular objective used. The exact agreement is, of course, fortuitous, but verifies the correctness of (12).

Wright (1923, p. 802) gave a more elaborate series of measurements of the same kind, although he did not explain exactly what he measured, and he described the results rather vaguely as "positions of extinction of

different points in the interference field." He did not compare his results with the predictions of a theory of the effect. The position $\psi = 45°$, $\theta_m = 57.6°$ at which I have measured δ_l corresponds to small circle coordinates $N = 36.6°$, $E = 36.6°$, as used by Wright; interpolating in his table (1923, p. 802), I find that he measured $\delta_l = 6.8°$, which is remarkably close to the average in Table 1.

To estimate ξ note that the effects of rotation due to equal refraction angles $\Delta\theta_i$ above and below the crystal plate under examination cancel, so that rotation produced by refraction at the surfaces of the crystal plate does not affect ξ, nor does the rotation produced by the glass slide and cover glass, if the two have the same index n. Moreover, since the front surface of the front objective lens element is plane, as is also the upper surface of the upper lens of the condenser, the effects of rotation at these two surfaces also cancel if the two lenses have the same index. If this index is about 1.5, the contribution of these surfaces to δ_l is close to δ_p. If there is a difference between δ_1 and δ_2, its maximum value is evidently

$$| \delta_2 - \delta_1 | \leq \delta_1 + \delta_2 - \delta_p = \delta_l - \delta_p \cong 2°.$$

Hence ξ is certainly no larger than about 1°, and very likely it is smaller, because it seems obvious that all of the remaining rotation is not produced solely in the objective or solely in the condenser. In section 8 it will be shown that ξ can be measured by means of interference figures, and the conclusion that ξ is less than 1° verified experimentally.

In the theory that follows (except in section 8) I shall assume that $\xi = 0$. When a given lens combination produces a significant value of ξ, the resulting effect on the position of the isogyres can be obtained by an obvious extension of the theory developed. For any point in the interference field

$$\xi = \frac{1}{2}(\delta_2 - \delta_1) = \frac{1}{2}\sin 2\psi \left\{ - \sum_{i=1}^{n_1} \sin^2 \frac{\Delta\theta_i}{2} + \sum_{i=n_1+1}^{n_1+n_2} \sin^2 \frac{\Delta\theta_i}{2} \right\}. \tag{14}$$

To the first approximation we can write

$$\Delta\theta_i = K_i\theta \tag{15}$$

where θ is the inclination in the crystal plate of the wave normal corresponding to a point P in the interference field with coordinates (θ, ψ). K_i is a constant for the i'th refracting surface. There are n_1 refracting surfaces in the condenser and n_2 in the objective. To the same approximation to which (15) is valid, $\sin^2\Delta\theta_i/2 = (\Delta\theta_i/2)^2$ so that (12) becomes

$$\xi = \frac{1}{2}\sin 2\psi \frac{\theta^2}{4}\left[- \sum_{1}^{n_1} K_i^2 + \sum_{n_1+1}^{n_1+n_2} K_i^2 \right].$$

The distribution of ξ values in the interference field is therefore, to the first approximation in θ,

$$\xi(\theta, \psi) = \xi_m \sin 2\psi \cdot \frac{\theta^2}{\theta_m^2} \tag{16}$$

ξ_m is the maximum value of ξ, the quantity estimated above.

Based on the assumption that ξ is 0, the isogyre theory I shall apply is contained in the following principle. At each point P in the interference field, imagine a cross to be drawn in the orientation given by a stereographic projection of the allowed directions of $\boldsymbol{D}$ drawn as a small cross on the reference sphere at the point corresponding to P. An isogyre passes through those points at which the crosses are aligned parallel to the NS and EW crosshairs of the microscope.

Note that Becke's construction would have given the same method of finding the position of the isogyres, if he had applied it in this way, instead of relying on the skiodrome theory. However, the assumption *behind* Becke's construction would *not* lead to the correct method. It is a case where an incorrect assumption and an incorrect construction lead to the correct conclusion.

6. *Uniaxial flash figures*

It is worthwhile to make a detailed application of the principle stated in the last section to the uniaxial flash figure, because for this figure the predictions of the theory can be compared precisely with the predictions of the skiodrome theory.

In applying the principle, it is easier and more direct to work with the reference sphere than to carry out the stereographic projection specifically. Fig. 8*a* is an orthographic view of the reference sphere, showing a point P defined by coordinates ϕ and $\rho = \sin\theta$, where θ is the inclination in the crystal plate of the wave normal $\boldsymbol{n}$ corresponding to P. PD_1 and PD_2 are drawn parallel to the arms of the stereographically projected $\boldsymbol{D}_1$, $\boldsymbol{D}_2$ cross corresponding to P. Fig. 8*b* is a stereographic projection of the same sphere. For a uniaxial crystal with optic axis emerging at A, the allowed directions of $\boldsymbol{D}$ at $\boldsymbol{n}$ are parallel and perpendicular, at $\boldsymbol{n}$, to the great circle $A\boldsymbol{n}$. In stereographic projection the angle γ, on the sphere, between $O\boldsymbol{n}$ (prolonged) and $\boldsymbol{n}A$ is preserved, because the stereographic projection is angle-true and the great circle $O\boldsymbol{n}$ projects as a line with the same azimuth ϕ. Thus in Fig. 8*a* the angle γ between PD_1 and OP (prolonged) can readily be calculated from spherical triangle $O\boldsymbol{n}A$ in Fig. 8*b*:

$$\cos\theta \cos\left(\frac{\pi}{2} - \phi\right) = -\sin\left(\frac{\pi}{2} - \phi\right) \cot(\pi - \gamma). \tag{17}$$

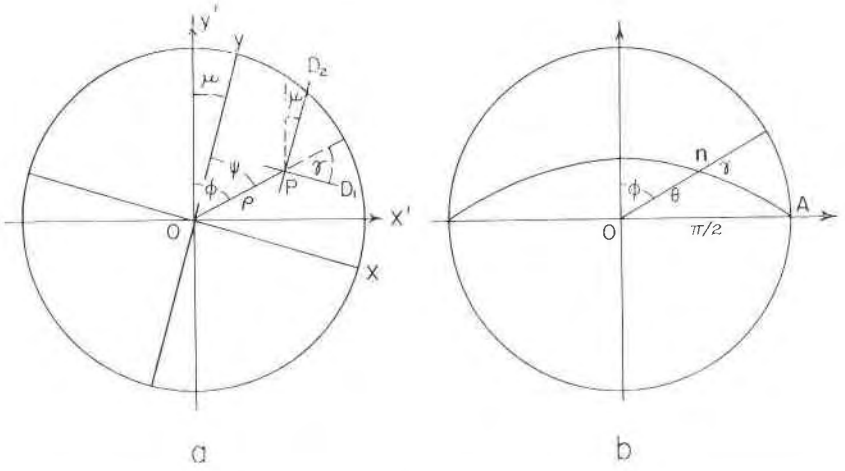

FIG. 8. Diagrams for analysis of the uniaxial flash figure. 8*a* represents the interference field (orthographic projection), and 8*b* is a stereographic projection of the interference hemisphere.

Now a given isogyre is traced out by all points P having a given inclination μ of the stereographically projected axes D_1, D_2 to the axes x', y':

$$\phi - \mu = \frac{\pi}{2} - \gamma. \tag{18}$$

Combining (17) and (18) we have for the equations of the isogyres

$$\tan(\phi - \mu) = \cos\theta \tan\phi \tag{19}$$

where μ is constant for a given isogyre.

(19) is written in coordinates (θ, ϕ) measured with respect to axes x', y' fixed in the crystal plate. If, as in most microscopes, the plate is rotated and the nicols remain fixed, it is more appropriate to describe the isogyres in terms of coordinates (θ, ψ) defined by the NS and EW cross hairs, which, for an isogyre passing through P, must be the x, y axes of Fig. 8*a*, so that

$$\psi = \phi - \mu \tag{20}$$

and the isogyre equation is

$$\tan(\psi + \mu) = \frac{\tan\psi}{\cos\theta}. \tag{21}$$

μ is the angle through which the crystal has been rotated from extinction.

To translate (21) into an equation describing the isogyre seen in the flash figure, it is necessary to introduce a relation between θ and radial distance ρ' from the center of the figure. If Mallard's law is valid, ρ' is

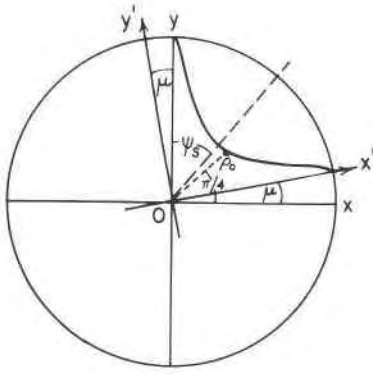

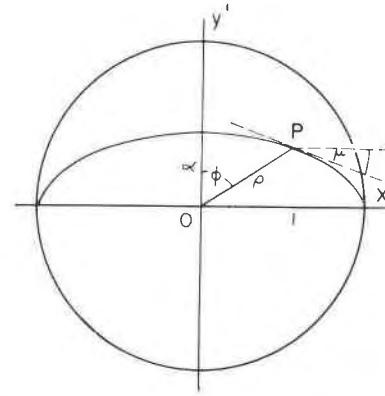

FIG. 9 (left). Form of the isogyre (heavy curve) in the uniaxial flash figure. The diagram is an orthographic projection of the entire interference hemisphere, of which only the inner part is visible in the conoscope. μ is exaggerated in the drawing.

FIG. 10 (right). Diagram for calculating the position of meridianal isogyres from the skiodrome theory for the uniaxial flash figure. The meridianal skiodrome passing through P is shown.

proportional to sin θ and hence to ρ in Fig. 8*a*, the proportionality constant depending, of course, on the microscope objective and the index of refraction of the crystal plate. I shall write the isogyre equations in terms of θ or ρ, realizing that these can always be converted to radial distance ρ' in the interference figure when needed.

The main features of an isogyre defined by equation (21) are plotted approximately in Fig. 9, which is an orthographic projection similar to Fig. 8*a*. The isogyre has a roughly hyperbolic shape. It passes through the optic axis at $x'=1$ and through the cross hair axis y at the edge of the sphere. The curve is mirror symmetric about the line $\psi=\psi_s=\pi/4-\mu/2$. Its closest approach to the center is along this line, and the derivative $d\rho/d\psi$ vanishes at the point of closest approach. $d\rho/d\psi$ is zero where the curve meets the edge of the sphere, but this affects only a small portion of the curve, as shown in Fig. 9. These features can be verified from equation (21).

Consider the shape of the isogyre near the center of the field for small angles of rotation μ. (21) can then be expanded:

$$(\tan\psi + \mu\sec^2\psi)(1 - \tfrac{1}{2}\rho^2) = \tan\psi$$

or

$$\rho^2 \sin 2\psi = 4\mu. \tag{22}$$

(22) is the equation of a rectangular hyperbola, as can be verified by substituting

$$x = \rho \sin \psi,$$
$$y = \rho \cos \psi.$$

As a quantitative test of eqn. (21), I shall use the angle μ_o required to bring the isogyre out to the edge of the interference field, defined by some angle θ_o and corresponding distance ρ_o. The isogyre actually disappears from the field along the line $\psi = \pi/4 - \mu/2$, but since μ_o is about 5° in practice this differs little from $\psi = \pi/4$. The distance ρ_o of the isogyre along $\psi = \pi/4$ is obtained by substituting this value in (21). After some simple reduction it is found to be given exactly by

$$2 \sin 2\mu_o = \frac{\rho_o^2}{1 - \frac{1}{2}\rho_o^2}. \tag{23}$$

Note that (22) agrees with (23) in the limiting case in which ρ_o and μ_o are small. The difference between θ_o calculated from (23) and θ_o' measured along $\psi = \pi/4 - \mu/2$ can be shown from (21) to be 0.05°, which is imperceptible. The change in μ required to move the isogyre from the position where it touches the edge of the field along $\psi = \pi/4$ to the position where it touches along $\psi = \pi/4 - \mu/2$ is 0.014°.

For comparison with (21), (22), and (23), the corresponding results for the meridianal isogyre given by the skiodrome theory will now be derived. The orthographically projected sphere is taken to have radius 1, as before. The meridianal skiodroms are ellipses, as shown in Fig. 10. α is a parameter defining the particular ellipse that passes through P. We have

$$x'^2 + \frac{y'^2}{\alpha^2} = 1$$
$$\tan p\mu = -\frac{dy'}{dx'} = \frac{x'}{y'}\alpha^2 = \alpha^2 \tan \phi.$$

Now put

$$x' = \rho \sin \phi$$
$$y' = \rho \cos \phi.$$

Then

$$\rho^2 \sin^2 \phi + \frac{\rho^2 \cos^2 \phi}{\tan \mu} \tan \phi = 1$$

or

$$\tan \mu = \frac{\rho^2 \sin 2\phi}{2(1 - \rho^2 \sin^2 \phi)}.$$

To write the result in cross hair coordinates, substitute (20) to get

$$\tan \mu = \frac{\rho^2 \sin 2(\psi + \mu)}{2(1 - \rho^2 \sin^2 (\psi + \mu))}. \tag{24}$$

(24) is the skiodrome equivalent of (21). Near the center of the field, where ρ is small, and μ must be small for the isogyre to be visible, (24) reduces to

$$2\mu = \rho^2 \sin 2\psi, \tag{25}$$

a rectangular hyperbola that is to be compared with (22). The meridianal isogyre reaches a given point in the interference field only after a rotation μ twice as great as the isogyre described by (22). Thus even at the center of the field the predictions of the two theories differ by a factor of 2.

For $\psi = \pi/4 - \mu$ (24) reduces to

$$2 \tan \mu_o = \frac{\rho_0^2}{1 - \frac{1}{2}\rho_0^2}. \tag{26}$$

(26) is also very nearly true for $\psi = \pi/4$, so that it is the skiodrome equivalent of (23).

A test between the two theories can best be made on the basis of (23) and (26). Note that (24) predicts a slightly larger value of μ_o than does (26), so that it accentuates the difference between the values of μ_o given by (23) and (26).

The results of a series of measurements of μ_o for flash figures in oriented mineral sections is given in Table 2. Each value reported is the mean of about 30 measurements for a given point in a given thin section. The "limit of error" values do not represent estimated standard errors of the

TABLE 2. SUMMARY OF FLASH FIGURE MEASUREMENTS
CONOSCOPE OF HALF APERTURE $\theta_m \cong 55°$

Mineral	n	μ_o values
Quartz	1.55	$4.4 \pm 0.6, 5.0 \pm 0.6, 4.8 \pm 0.6$ (av.) 4.7
Beryl	1.56	$3.7 \pm 0.3, 4.6 \pm 0.6, 4.0 \pm 0.7, 3.8 \pm 0.3, 5.7 \pm 0.8, 4.9 \pm 0.7,$ $4.6 \pm 0.6, 5.2 \pm 1.2$ (av.) 4.6
Apatite	1.64	$4.3 \pm 0.4, 3.5 \pm 0.4, 4.4 \pm 1.1, 4.3 \pm 0.8$ (av.) 4.1
Tourmaline	1.64	$4.5 \pm 1.7, 4.4 \pm 2.1, 3.5 \pm 1.1, 4.5 \pm 2.1$ (av.) 4.2

mean, but rather the maximum scatter of μ_o values obtained in each set of about 30 measurements. The means scatter more than one would have estimated from the scatter of the individual measurements, probably because of subjective effects of the kind mentioned in section 5, and also because of an effect discussed in section 8.

The measurements are made in the following way. Only nearly centered figures are measured. The azimuthal setting of the stage required

to place the isogyre at the edge of the field in each quadrant of the field is then measured five or six times, for rotation from a given extinction position. Finally several measurements are made of the azimuthal setting that produces the centered cross. The μ_o values are obtained afterwards, by difference. This procedure tends to eliminate advanced bias as to how the values should turn out. The final μ_o value, obtained by averaging the values from each equadrant, tends to eliminate the effects of slight misorientation of the section.

In making the measurements, the object is to set the center of the isogyre at the edge of the field. This is made difficult and somewhat uncertain by the fact that when set properly, only one edge of the isogyre can be seen. It is necessary to swing the stage back and forth through the correct position in order to make sure where the center of the isogyre is. The flash figure isogyre is rather diffuse, so that the settings cannot be made very accurately. It might be preferable to make the settings for a ρ_o value within the field of the conoscope, as could be done with an ocular provided with a circular reference hair. Such an ocular was not available, but in addition I considered it desirable to make the measurements at the largest possible value of ρ_o, for which the μ_o values predicted by (23) and (26) differ most.

Before beginning the measurements, I estimated from standard *Bxa* slides that the conoscope used (see section 5) has a half-aperture in air, which I will call θ_m, of about 55°. For a mineral with index $n=1.56$, the interference sphere can therefore be seen out to $\theta_o=31.9°$, and for $n=1.64$, $\theta_o=30.0°$. Equations (23) and (26) then predict the μ_o values shown in Table 3.

TABLE 3. COMPARISON OF CALCULATED AND OBSERVED μ_0 VALUES FOR FLASH FIGURES. $\theta_m=55°$

n	μ_o (23)	μ_o (26)	μ_{obs} (av.)
1.56	4.6°	9.1°	4.6°, 4.7°
1.64	4.1°	8.1°	4.1°, 4.2°

The observed values are the averages from Table 2 for each of the four minerals. It is clear that (23) accounts for the observed values and (26) does not. To obtain agreement between (26) and the observed values it would be necessary to assume $\theta_m=37.8°$, whereas the isogyres in 45° position in a centered *Bxa* figure of muscovite, with $E=39°$, are well within the field of the conoscope.

The measurements of *Bxa* and *Bxo* figures, given in the next section, suggest that the correct value of θ_m for the conoscope used is about

57.6°, slightly larger than the value used in Table 3. The numerical aperture 0.85 of the objective, stated by the manufacturer, corresponds to $\theta_m = 58.2°$. This value gives calculated μ_o values somewhat larger than those listed in Table 3 (e.g., $\mu_o(23) = 5.1°$ for $n = 1.55$). Students who have made flash figure measurements for me generally find somewhat higher μ_{obs} values also, for lenses of the same rated N.A. as the one I used.

At first I was cautious not to rely on the accuracy of the conoscopic angles and numerical apertures stated by lens manufacturers, but the close agreement between μ_o values actually measured and μ_o values calculated from the theory by assuming the correctness of the rated numerical apertures shows that this caution is unnecessary. Several examples of the agreement will be seen in sections 7 and 8. For any lens for which the numerical aperture in air,

$$\text{N.A.} = n_{\text{air}} \sin \theta_m \cong \sin \theta_m = \rho_m,$$

is accurately known, isogyre calculations can be readily made by taking

$$\rho_o = \frac{\rho_m}{n}$$

where n is the index of refraction of the crystal plate.

7. *Acute and Obtuse Bisectrix Figures*

The analysis of *Bxa* and *Bxo* figures can be carried out by the methods used in the last section, with the help of Fig. 11. Angles α_1, α_2 and γ can be introduced as shown, and the inclination μ calculated from the law of Biot and Fresnel. I shall not write down the details of the derivation, but simply state the result, converted to cross-hair coordinates θ and ψ, as defined by (20):

$$\cot 2\psi \sin 2(\psi + \mu) \cos \theta + \sin^2 (\psi + \mu)(2 - \sin^2 \theta) = 1 + \sin^2 \theta \cot^2 V. \quad (27)$$

The result is cumbersome, but can be simplified in two ways. If we suppose that θ is small enough that to a sufficiently good approximation

$$\cos \theta = 1 - \tfrac{1}{2}\rho^2$$

then one can show, after some calculation, that (27) reduces to the simple form

$$\frac{\rho_1^2}{1 - \frac{1}{2}\rho_1^2} \sin 2\mu = \frac{\rho^2}{1 - \frac{1}{2}\rho^2} \sin 2\psi, \quad (28)$$

where

$$\rho_1 = \sin V$$

and, as before,

$$\rho = \sin \theta.$$

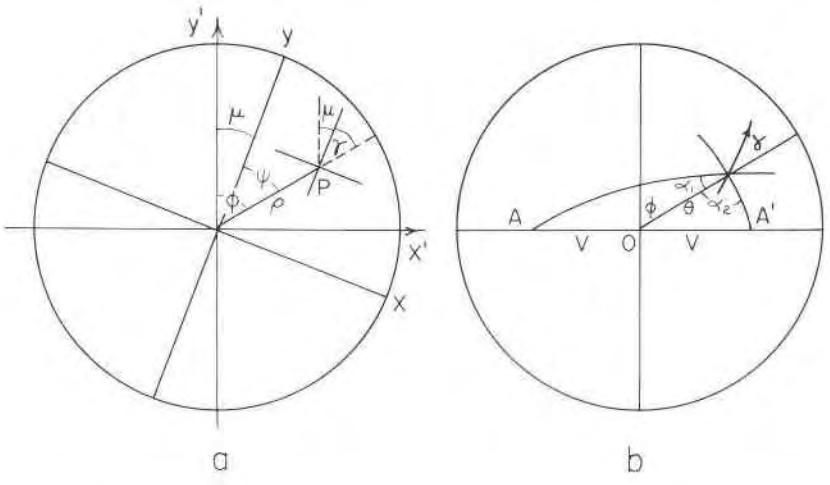

FIG. 11. Diagrams for analysis of centered *Bxa* and *Bxo* figures. In 11*b* the optic axes project to the points *A* and *A'*. 11*a* represents the interference field (orthographic projection), and 11*b* is a stereographic projection of the interference hemisphere.

(28) describes a curve that approaches the shape of a rectangular hyperbola for small ρ. Its closest approach to the center is along the line $\psi = \pi/4$.

A second simplification is to evaluate (27) for $\psi = \pi/4$. It then reduces exactly to

$$\frac{{\rho_1}^2}{1 - \frac{1}{2}{\rho_1}^2} \sin 2\mu_o = \frac{{\rho_0}^2}{1 - \frac{1}{2}{\rho_0}^2}. \tag{29}$$

Note that (28) yields (29) when $\psi = \pi/4$, and that (29) reduces to (23) when $\rho_1 = 1$ (uniaxial flash figure). Since the exact shape of the isogyre, as given by (27), is not important in practice, I will make use only of (29) in applications of the theory.

The relationship between (28) and (29) makes possible a fairly simple evaluation of the deviation of (27) from (28). The two curves evidently intersect at $\rho = \rho_o$, $\psi = \pi/4$. The slope $d\theta/d\psi$ at this point is found to be

$$\frac{d\theta}{d\psi} = \frac{2 \cos 2\mu_o}{\cos \theta_o (1 + \sin 2\mu_o + 2 \cot^2 V)} (1 - \tfrac{1}{2}{\rho_0}^2 - \sqrt{1 - {\rho_0}^2}).$$

The slope is greatest for the uniaxial flash figure (for which it is 0.036), and decreases steadily as V decreases and μ_o increases, becoming zero for $\mu_o = 45°$ ($V = \theta_o$). This conclusion seems to violate what is observed in practice, that for figures with μ_o about 15° or greater, the slope $d\theta/d\psi$ of the isogyre at $\psi = \pi/4$ appears to become noticeable. However, I think the apparent slope is exaggerated by the rapid fanning out of the iso-

gyre near the optic axes, which are near the edge of the field in such figures.

Because of the importance of $\rho^2/1-\frac{1}{2}\rho^2$ in (28) and (29), the function is plotted againt θ in Fig. 12. In Fig. 13 are shown curves giving μ_o as a function of V, from (29), for various values of the mean index n of the

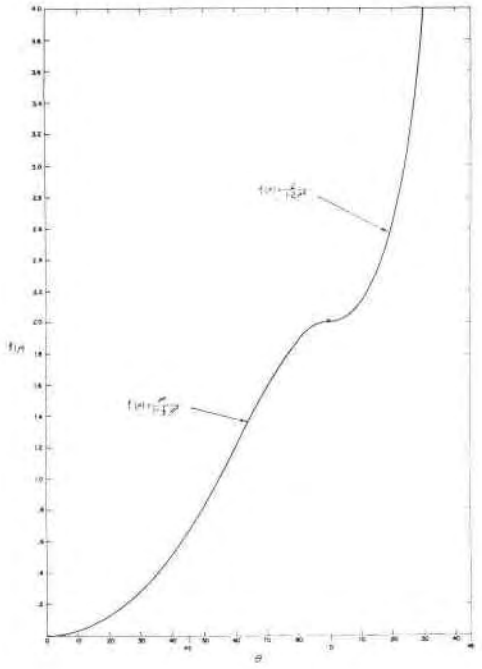

FIG. 12. The functions $f(\rho)=\rho^2/1-\frac{1}{2}\rho^2$ and $f(\rho)=2/1-2\rho^2$ plotted against θ.

crystal plate. The conoscope half aperture θ_m is assumed to be 57.6° in the calculation of these curves. Each curve corresponds to a given value of θ_o, as shown in Table 4, so that the curves can be adapted to conoscopes of different aperture by using the relation (Snell's Law)

$$n \sin \theta_o = \sin \theta_m. \tag{30}$$

Equation (29) and the curves of Fig. 13 provide a means of measuring

TABLE 4. PARAMETERS FOR THE CURVES IN FIG. 13

Curve	1	2	3	4	5
θ_0	33.1°	31.9°	30.8°	29.8°	28.8°
$\rho_0^2/1-\frac{1}{2}\rho_0^2$	.351	.326	.302	.281	.261
n	1.55	1.60	1.65	1.70	1.76

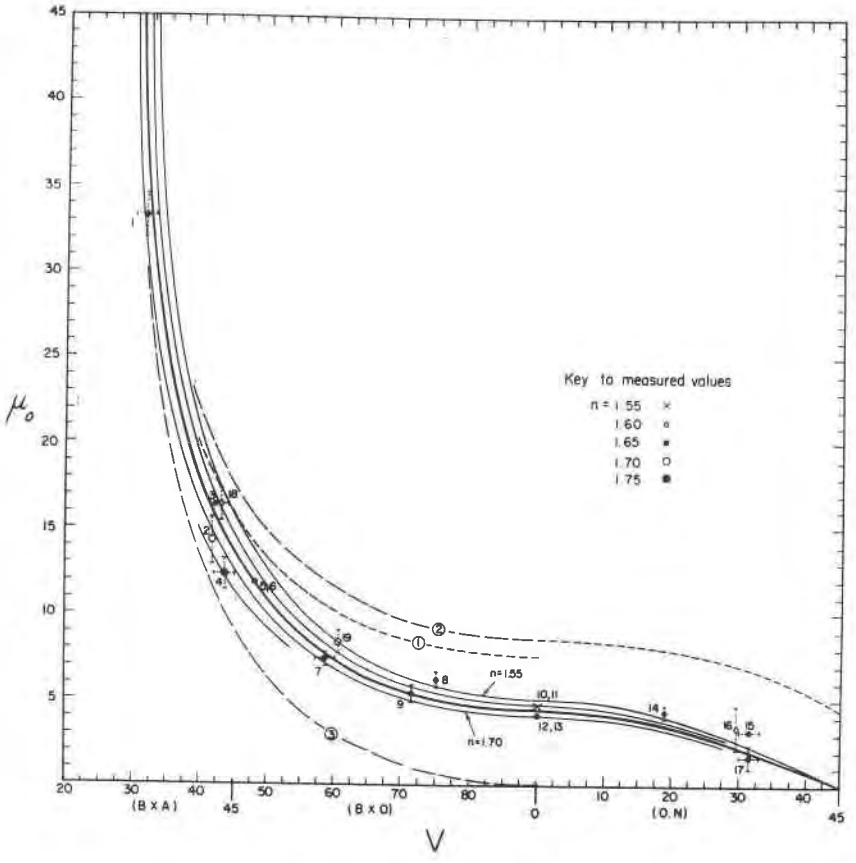

FIG. 13. Comparison of theoretical curves of μ_0 as a function of V with measured μ values from oriented thin sections. Conoscope is assumed to have half aperture $\theta_m = 57.6^\circ$ (N.A. 0.845) for the theoretical curves, which are calculated for crystal plate indices of refraction varying from 1.55 to 1.70 in intervals of 0.05. The curve for $n = 1.65$ is drawn with a heavy line, and is to be compared with dashed curve (1), given by the theory of Michel-Lévy for the same index and aperture, and with curves (2) and (3), from the skiodrome theory. The plotted points are identified by number in Table 5, and by index in the key on the figure.

V in *Bxa* and *Bxo* figures, and in particular a means of distinguishing between *Bxa* and *Bxo* figures. The method was first proposed by Michel-Lévy (1888) but his theoretical treatment of the method was not satisfactory. Curve 1 (dashed) in Fig. 13 shows the angles μ_o given by his theory for $n = 1.65$. $\theta_m = 57.6°$. The curve is calculated from the isogyre equation

$$\rho^2 \sin 2\psi = \rho_1^2 \sin 2\mu \tag{31}$$

by putting $\psi = \pi/4$, $\rho = \rho_o$, $\mu = \mu_o$.

A derivation of (31) can be found in Wright's paper (1905, p. 288) or in Johannsen's text (1918, p. 441).

Curves 2 and 3 are derived from the isogyres of the skiodrome theory. The calculation of skiodrome isogyre shapes is cumbersome, but simplifies for $\psi = \pi/4$ to the relationships

$$\rho_1^2 = \frac{\rho_o^2}{\sin 2\mu_o \left[1 - \frac{1}{2}\rho_o^2(1 - \tan \mu_o)\right]} \tag{32a}$$

$$\rho_1^2 = \frac{\rho_o^2}{\sin 2\mu_o \left[1 + \frac{1}{2}\rho_o^2(\cot \mu_o - 1)\right]}. \tag{32b}$$

(32*a*) gives curve 2, which corresponds to the meridianal isogyre for $V > 45°$, while (32*b*) gives curve 3 (Fig. 13).

To test the various theories, I have measured angles μ_o for a number of *Bxo* figures, and *Bxa* figures of large $2V$, obtained from oriented thin sections. The points are plotted in Fig. 13. The measurements were made in the way described in section 6 for uniaxial flash figures. Values of V are averages of data given by Winchell (1951) and Tröger (1956). I have avoided minerals for which a wide range of V is reported. Note that the points in Fig. 13 are identified by index n and by a reference number, which refers to the summary in Table 5. Rough "limit of error" brackets have been added to those points in Fig. 13 for which the uncertainty in measured μ_o values or in V values quoted in the literature is important.

The measurements confirm the applicability of (29). Best overall agreement with the calculated curves is obtained by taking $\theta_m = 57.6°$. Points 14–17 were omitted in the comparison.

The averages of the μ_o values given by curves 2 and 3 in Fig. 13, for given values of V, reproduce rather closely the μ_o values calculated from (29). In this sense the skiodrome theory is "on the average" correct, which can be understood from the way the $\boldsymbol{D}_1$, $\boldsymbol{D}_2$ cross behaves when orthographically projected. Nevertheless, the skiodrome theory itself has no means of predicting what sort of averaging of the μ_o values should give the correct result, and the use of (32) and (33), with averaging, is, of course, more cumbersome than direct application of (29).

In Fig. 14 are given curves of μ_o against V calculated from (29) for values of n ranging from 1.45 (curve 1) to 1.80 (curve 8). The curves 1 to 8 are for an objective of N.A. 0.85, and the curves *a* to *h* for N.A. 0.65, these being the numerical apertures of standard objectives used in conoscopic work. The larger aperture is clearly advantageous. For example, the reliability with which a figure can be distinguished as *Bxa* or *Bxo* increases with the (magnitude of) the slope of the μ_o vs. V curve at $V = 45°$.

It is advisable before using the curves of Fig. 14 to check the N.A. of the objective used. This can conveniently be done, and the applicability

TABLE 5. MEASURED DATA PLOTTED IN FIG. 13. LIMIT OF ERROR IS (ROUGHLY) ESTIMATED STANDARD DEVIATION OF MEAN. OBJECTIVE OF N.A. 0.85 (Leitz No. 7)

Point Ref. No.	Mineral	Sec.	n	μ_0 (measured)	V (lit.)
1	Topaz	*Bxa*	1.63	33.2±1.3	30 –33
2	Kyanite	*Bxa*	1.72	14.3±1.4	41.7
3	Andalusite	*Bxa*	1.64	16.4±0.1	41.5–42.5
4	Staurolite	*Bxa*	1.75	12.3±0.9	42 –45
5	Andalusite	*Bxo*	1.64	11.8±0.1	41.5–42.5
6	Andalusite	*Bxo*	1.64	11.9±0.3	41.5–42.5
7	(F−) Topaz	*Bxo*	1.63	7.4±0.4	30 –33
8	Sillimanite	*Bxo*	1.67	5.9±0.5	12.5–15
9	Barite	*Bxo*	1.64	5.4±0.5	18.7
10	Quartz	flash	1.55	4.7±0.2	0
11	Beryl	flash	1.56	4.6±0.2	0
12	Apatite	flash	1.64	4.1±0.2	0
13	Tourmaline	flash	1.64	4.2±0.2	0
14	Barite	o.n.	1.64	4.3±0.4	18.7
15	Topaz	o.n.	1.63	3.2±0.2	30 –33
16	Augite	o.n.	1.70	3.4±1.3	29.5
17	Topaz	o.n.	1.63	1.7±0.7	30 –33
18	Tremolite	*Bxa* (poorly centered)	1.61	16.4±1.0	42? –44
19	Augite	*Bxo*	1.69	8.2±0.7	29.5

of the theory also tested, by measuring μ_o for *Bxa* and *Bxo* figures of andalusite ($V=42°$ and 48°), plotting the measured points on Fig. 14, and checking that they fall at places appropriate to $n=1.64$. If the objective has numerical aperture (ρ_m) other than 0.85 or 0.65, the curves of Fig. 14 can be adapted to it by assigning new values of n by the relation (30). The ρ_o values for the curves of Fig. 14 are given in Table 6. If ρ_m for an objective is unknown, it can be determined by reversing the above procedure, or also, of course, by using a stage apertometer.

8. The effect of non-zero ξ

Although ξ (section 5) is small, so that the isogyre equations for $\xi=0$ give a good representation of observed interference figures, an actual non-zero value of ξ has a small but definite effect on the μ_o values measured. It can be seen from Fig. 11, or from diagrams of the kind shown in Fig. 19, that if μ_o is measured by rotating the crystal plate from the extinction position where the optic plane is NS, then a positive value of ξ, as defined in eqn. (9) and Fig. 7*a*, tends to reduce the measured μ_o value from the value predicted for $\xi=0$. Call the μ_o value meas-

ured in this way μ_V, and call the value measured about the extinction position with the optic plane EW μ_H. If ξ is positive, then μ_V is less than μ_o, the value expected for $\xi=0$, but μ_H is greater than μ_o. A detailed analysis of this situation would be required if ξ were large. Instead, since

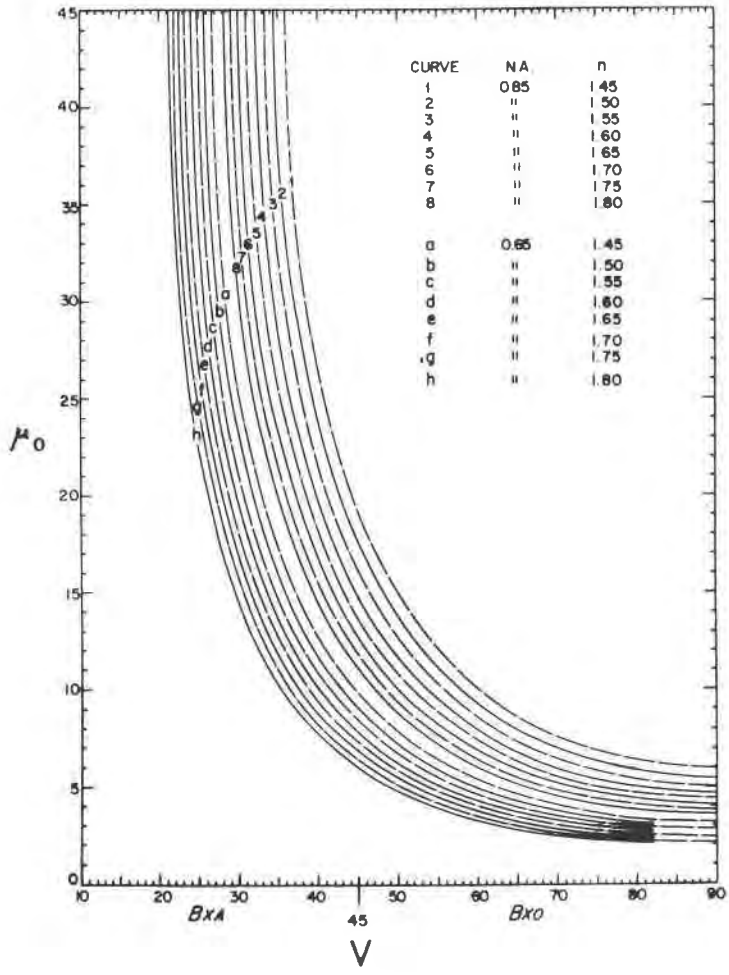

FIG. 14. Theoretical curves of μ_0 against V for conoscopes of N.A. 0.85 (numbered curves) and N.A. 0.65 (lettered curves). The curves are calculated for crystals of mean index of refraction ranging from 1.45 to 1.80 at intervals of 0.05, as indicated.

ξ is small, then if μ, regarded as a function of ψ for constant $\theta=\theta_o$ in eqn. (27), varies much less rapidly than ψ itself, as is true for the *Bxa* and *Bxo* figures considered above, we may write (to first order in ξ_m)

TABLE 6. DATA FOR CURVES OF FIGURE 14

N.A.	Curve	n	θ_0	ρ_0	$\frac{\rho_0^2}{1-\frac{1}{2}\rho_0^2}$
0.85	1	1.45	35.9°	0.586	0.415
	2	1.50	34.5	.566	.382
	3	1.55	33.3	.548	.354
	4	1.60	32.1	.531	.328
	5	1.65	31.0	.515	.306
	6	1.70	30.0	.500	.285
	7	1.75	29.1	.486	.267
	8	1.80	28.2	.472	.251
0.65	*a*	1.45	26.6	.448	.223
	b	1.50	25.7	.433	.207
	c	1.55	24.8	.419	.193
	d	1.60	24.0	.406	.180
	e	1.65	23.2	.394	.168
	f	1.70	22.5	.382	.158
	g	1.75	21.8	.371	.148
	h	1.80	21.2	.361	.139

$$\mu_V = \mu_o - \xi_m$$
$$\mu_H = \mu_o + \xi_m \qquad (33a)$$

where ξ_m is the value of ξ at $\psi = \pi/4$, $\theta = \theta_o$ (eqn. (16)).

Thus for a given figure μ_o and ξ_m can be determined by measuring μ_V μ_H:

$$\mu_o = \tfrac{1}{2}(\mu_V + \mu_H) \qquad (33b)$$
$$\xi_m = \tfrac{1}{2}(\mu_H - \mu a) \qquad (33c)$$

To test the above conclusions, I have made a careful series of measurements on three figures: andalusite *Bxa*, andalusite *Bxo*, and quartz flash, for which the data are given in Table 7. The figures were measured with a Zeiss model GFL668-666 petrographic microscope, using objective "Pol 50/0.85" of N.A. 0.85. The scatter in ξ_m values calculated from (33c) is probably mainly random, though ξ_m may be affected by the slides themselves, if slide and cover glass have different indices. Evidently ξ_m is about $-0.7°$ for the lens combination used. The measured μ_o values, obtained from (33*b*), agree excellently with the values calculated from the theory (eqn. (29)) by assuming $\rho_m = 0.85$ and assuming $V = 42°$ for andalusite. I consider the data of Table 7 to be the most definitive test of the theory, because the measurements reported in Tables 2 and 5 were made before I was aware of the proper way to take a nonzero ξ into account, and they were made with an inferior microscope.

TABLE 7. INTERFERENCE FIGURE MEASUREMENTS WITH ZEISS MODEL GFL668-666, OBJECTIVE "Pol 50/0.85," OF N.A. 0.85

Extinction setting	Optic plane set	Isogyre in quadrant	Andalusite Bxa		Andalusite Bxo		Quartz Flash	
			μ_V	μ_H	μ_V	μ_H	μ_V	μ_H
1	NS	1	16.3	—	12.7	—	5.6	—
		2	15.7	—	11.0	—	6.7	—
		3	18.0	—	12.7	—	5.0	—
		4	15.7	—	14.7	—	6.8	—
2	EW	1	—	15.2	—	9.8	—	3.8
		2	—	14.3	—	11.5	—	4.9
		3	—	16.0	—	11.9	—	4.8
		4	—	16.1	—	11.6	—	4.4
3	NS	1	18.5	—	13.3	—	5.1	—
		2	16.3	—	14.0	—	5.7	—
		3	15.9	—	14.0	—	5.4	—
		4	16.3	—	10.8	—	6.3	—
4	EW	1	—	15.7	—	12.1	—	4.9
		2	—	16.9	—	11.6	—	4.2
		3	—	15.7	—	10.2	—	3.7
		4	—	13.4	—	10.5	—	4.7
Average μ_V and μ_H			16.6	15.4	12.9	11.1	5.8	4.4
ξ_m from (33*c*)			−0.6		−0.9		−0.7	
μ_0 from (33*b*)			16.0		12.0		5.1	
μ_0 from (29)			16.1		12.0		5.1	

The important conclusion to be drawn is that in measuring *Bxa* and *Bxo* figures, the effect of a small non-zero ξ is eliminated by averaging μ_V and μ_H.

9. Optic Normal Figures

Equations of the optic normal isogyres can be obtained with the help of Fig. 15. The rather unwieldy result is

$$2 \cot 2\psi \cos\theta \sin 2(\psi - \mu) - (2 - \sin^2\theta) \cos 2(\psi - \mu) + \sin^2\theta \cos 2V = 0 \quad (34)$$

(34) simplifies for $\psi = \pi/4$ to

$$2 \sin 2\mu_0 = \frac{{\rho_0}^2}{1 - \frac{1}{2}{\rho_0}^2} \cos 2V$$

or

$$\frac{2}{1-2\rho_1^2}\sin 2\mu_0 = \frac{\rho_0^2}{1-\frac{1}{2}\rho_0^2}. \tag{35}$$

Note that when $\rho_1 = 0$ (uniaxial flash figure), (35) reduces to (32).

In Fig. 13 (35) is plotted as a continuation of the μ_o vs. V curves, with a new origin for the V coordinate. The angle μ_o for a "neutral" figure with $2V = 90°$ is 0, meaning that the cross does not break up into hyperbolae as the crystal is rotated from extinction.

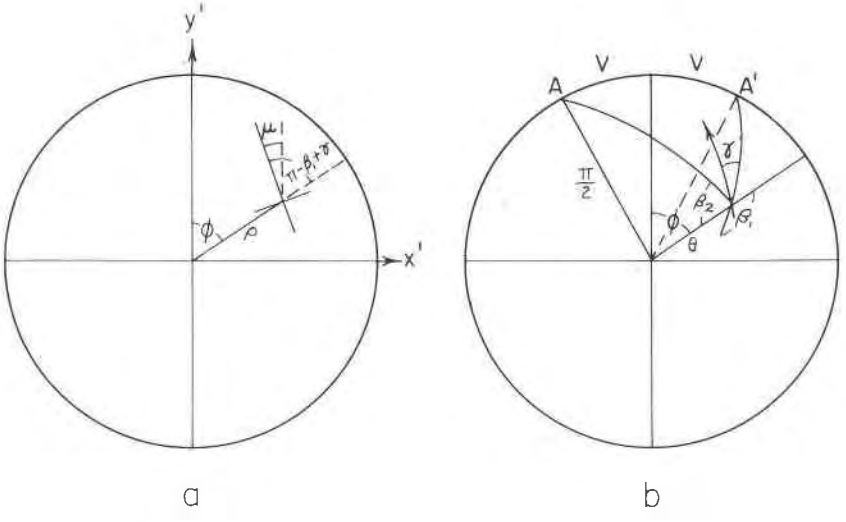

FIG. 15. Diagrams for analysis of optic normal figures. 15*a* represents the interference field (orthographic projection), and 15*b* is a stereographic projection of the interference hemisphere.

Most of the measured μ_o values for optic normal figures lie above the curves of Fig. 13. The figures are difficult to measure with any accuracy because the isogyres are so diffuse, and it therefore seems that a detailed comparison with the other theories is not of much value over this range. Michel-Lévy's equation cannot logically be extended to optic normal figures. I have bothered to analyze the skiodrome theory only for $V = 45°$, where it predicts two points at an equal distance above and below the $\mu_o = 0$ axis, corresponding to the continuation of curves 2 and 3 of Fig. 13. The predicted value of μ_o is given exactly by

$$\frac{\tan \mu_o}{1-\tan^2 \mu_o} = \frac{\rho_o^2}{4(1-\frac{1}{2}\rho_o^2)} \tag{36}$$

Since μ_o is small, the value given by (36) is just half the value predicted by the skiodrome theory for uniaxial flash figures, eqn. (26). It is plotted

as a point in Fig. 13, and curve 2 is connected across schematically from $V=0$ to $V=45°$.

10. Optic Axis Figures

As a last application of the theory, it is interesting to compare its predictions with those of Wright (1905, 1907) for optic axis figures. In the 1905 paper Wright gave a series of curves showing the appearance of the

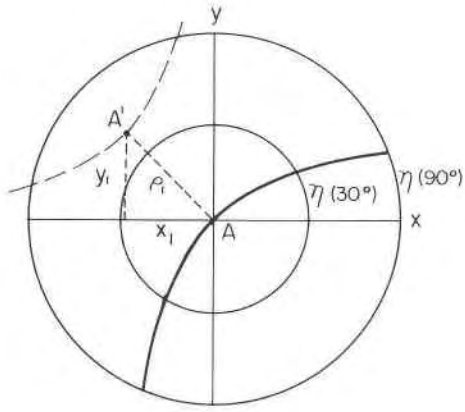

FIG. 16. Orthographic projection of the interference hemisphere for the optic axis figure. The optic axis is at A, and the heavy line shows the position of the isogyre in the 45° setting. The second optic axis is shown schematically at A', as envisaged in Wright's derivation of the isogyre equation.

optic axis isogyres in the 45° position. The curves were computed from the equation

$$xy + \tfrac{1}{2}x_1(y - x) = 0 \tag{37}$$

where x, y are coordinates (in the interference field) of points on the isogyre and x_1 is the x-coordinate of the second optic axis, which may or may not be in the interference field, as shown in Fig. 16 (note that $x_1=y_1$). (37) is derived by applying a planar analog of the law of Biot and Fresnel to the plane of Fig. 16, and is thus the optic axis figure analog of Michel-Lévy's equation, (31). To be consistent, one would assume that the points (x, y) and (x_1, y_1) represent an orthographic projection of the interference sphere. However, Wright assumed the projection to be gnomonic in calculating his isogyre curves. The only justification for such an assumption, as far as I can see, is that it gives the correct type of isogyre (a straight line) for $2V=90°$, which an orthographic projection would not.

In his 1907 paper, Wright superseded the earlier curves with a new set, apparently determined from the skiodrome theory. Nevertheless, the older curves have found their way into optical mineralogy texts and the newer ones not, perhaps because the newer curves do not look much like the isogyres actually seen in interference figures.

The present theory may be applied by using Fig. 17. Written in co-

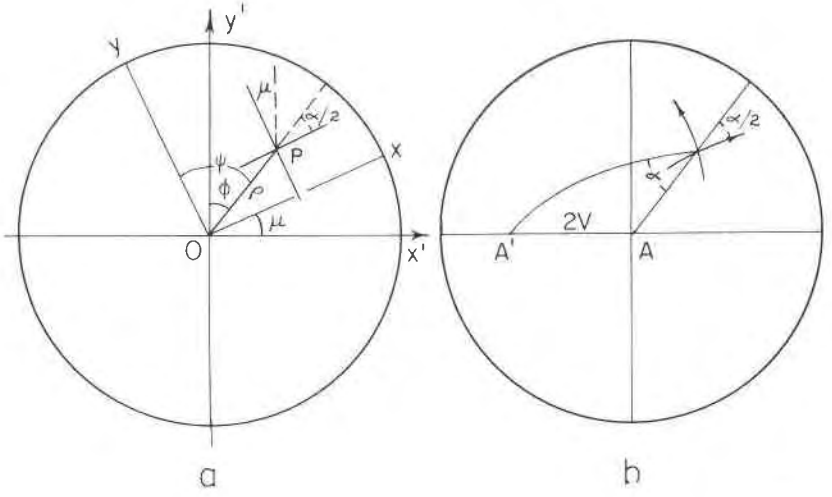

FIG. 17. Diagrams for analysis of optic axis figures. 17*a* represents the interference field (orthographic projection), and 17*b* is a stereographic projection of the interference hemisphere.

ordinates (θ, ψ) measured with respect to the cross-hair axes x, y, the isogyre equation is

$$\sin\theta \cot 2V + \cos\theta \sin(\psi - \mu) - \cot 2\psi \cos(\psi - \mu) = 0. \tag{38}$$

For the isogyre in the 45° position, put $\mu = \pi/4$ in (38); the isogyre then has the form shown by the solid curve in Fig. 16. A good test of Wright's curves (1905, p. 291) is to compare the angle η (Fig. 16) at the periphery of the field (which Wright chose as $\theta_o = 30°$) with the corresponding values calculated from (38).

Since $\eta = \pi/2 - \psi$, (38) becomes

$$\tan 2V = \frac{\sin\theta}{\cot 2\eta \cos\left(\frac{\pi}{4} - \eta\right) - \cos\theta \sin\left(\frac{\pi}{4} - \eta\right)} \tag{39}$$

from which values of V can be calculated for a series of η values, at a given value of θ. A curve for $\theta = 30°$ is plotted in Fig. 18. Note that, to a

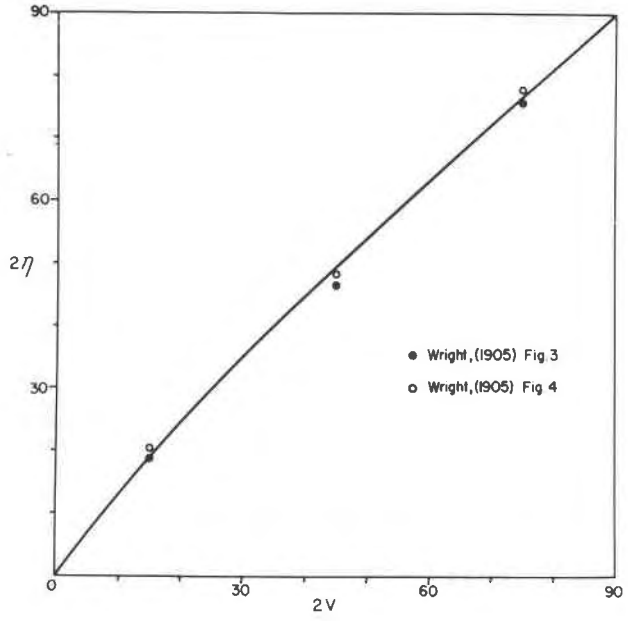

FIG. 18. Curve showing 2η (30°) as a function of $2V$, from equation (39). For comparison are plotted values measured from Wright's isogyre curves (1905, Figs. 3 and 4).

good approximation, $\eta \cong V$, a fact that may be convenient to remember. Plotted also in Fig. 18 are points measured from Wright's (1905) Fig. 3 and Fig. 4. The agreement is remarkably close, certainly well within the accuracy needed for practical work.

This unexpected agreement has an interesting explanation. If we suppose the interference sphere to be orthographically projected, so that

$$x = \rho \sin \psi, \qquad y = \rho \cos \psi,$$
$$x^2 + y^2 = \rho^2, \qquad \rho = \sin \theta,$$

then (38) becomes, in cartesian coordinates, and with $\mu = \pi/4$:

$$(x^2 - y^2)(x + y) - 2\sqrt{2}\rho^2 xy \cot 2V - 2\sqrt{1 - \rho^2}(x - y)xy = 0 \qquad (40)$$

(40) is to be compared with Wright's equation, (37).
In case ρ is small enough that we can write

$$\sqrt{1 - \rho^2} = 1 - \tfrac{1}{2}\rho^2$$

then (40) reduces to

$$(x - y)(1 + xy) - 2\sqrt{2}\, xy \cot 2V = 0. \qquad (41)$$

This is of the same form as (37), except for the factor $(1+xy)$. The factor is always near 1 for points in the conoscope field, where xy has a

maximum value of 1/4. Hence (41) is approximated by

$$xy + \frac{\tan 2V}{2\sqrt{2}}(y - x) = 0 \tag{42}$$

which is a rectangular hyperbola passing through the origin.

Now if (37) were a plot in gnomonic projection, with the plane of projection tangent to the unit sphere about the projection point, presumably this would mean taking

$$x_1 = \rho_1 \sin \psi = \frac{\tan 2V}{\sqrt{2}}$$

and this substitution makes (37) and (42) identical. This is the reason for the close agreement between Wright's curves and the predictions of (39). It seems remarkable that the gnomonic projection of a sphere that should be orthographically projected, combined with the planar analog of a law that applies to the surface of a sphere, should yield a result so nearly correct. It seems unlikely that there is anything specially suitable about the gnomonic projection, because the substitution $\rho_1 = \tan V$ in Michel-Levy's equation, (31), does not yield the correct result, (28).

11. Summary and Conclusion

The most useful result obtained with the present theory is a relation from which $2V$ can be measured in centered *Bxa* figures of large $2V$, and in centered *Bxo* figures. One measures the angle of stage rotation μ_o required to disperse the isogyres from a centered cross (extinction) to the edge of the interference field of radius

$$\rho_o = \sin \theta_o = \frac{\sin \theta_m}{n} = \frac{\rho_m}{n}$$

where θ_m is the half-aperture of the conoscope in air and n is the average index of refraction of the mineral examined. ρ_m is the numerical aperture of the objective lens. μ_o is then related to $\rho_1 = \sin V$ by

$$\frac{\rho_o^2}{1 - \frac{1}{2}\rho_o^2} = \frac{\rho_1^2}{1 - \frac{1}{2}\rho_1^2} \sin 2\mu_o$$

which is plotted in Fig. 14 for N.A. 0.85 and 0.65, and various values of n. Experimental verification of this relation is considered a verification of the theory here used. The relation does not depend on the validity of Mallard's law. It provides in particular a means for distinguishing between *Bxa* and *Bxo* figures.

An important practical feature of the theory is that, although the effect on isogyre position of the much-debated "rotation" of the polarization plane in the conoscope is small but definite, it can be entirely

eliminated from the measurements simply by averaging the μ_o values obtained by turning from the two extinction positions (optic plane NS or EW).

An application of the theory to the optic axis figure shows that the 45° isogyre curves derived by Wright (1905) are very nearly correct, quite good enough for practical work. This seems remarkable, in view of the peculiar assumptions made in Wright's derivation of the curves.

The skiodrome theory gives incorrect isogyres, significantly incorrect even near the center of the field. Stereographic projection of the refer-

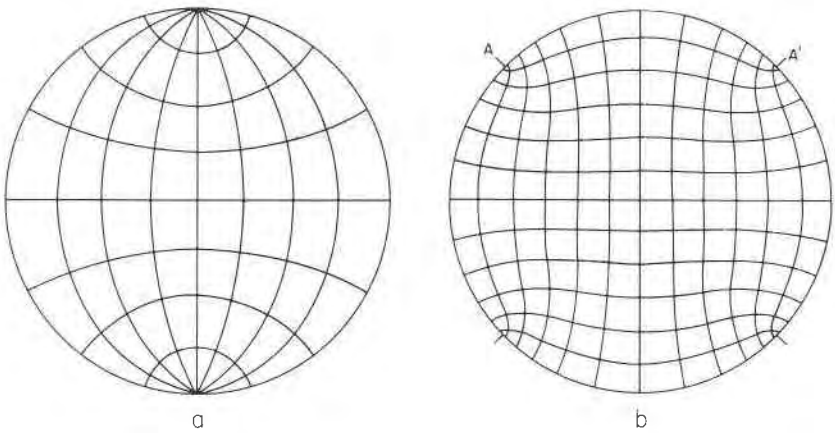

FIG. 19. "Extinction direction nets" for uniaxial flash figure (*a*) and optic normal figure with $2V=90°$ (*b*).

ence sphere would give a much better representation of the isogyre pattern. If the stereographic projection is carried out by the relation

$$\rho' = 1.945 \tan \theta/2$$

the radial distance ρ' will differ little from the radial distance

$$\rho = \sin \theta$$

for orthogonal projection of the interference sphere, within the field of practical conoscopes ($\theta < 30°$). The outer portion of the stereographically projected pattern would be enlarged, but this part is never seen anyway.

The main advantage of the skiodrome is that the projected isotaques are easily calculated, at least when projected on the principal planes, where they are ellipses or hyperbolae. The same advantage probably will not accure to the stereographically projected curves. In principal it is possible to calculate the two orthogonal sets of curves of a net which would correctly represent the isogyres in the orthogonally projected in-

terference sphere, according to the theory here developed. However, for quantitative purposes the direct approach used in this paper is more useful, and for qualitative purposes, as in teaching, a diagram can be drawn from qualitative considerations that shows all the features that are important, without the need of resorting to exact calculation of the net. Thus Fig. 19*a* represents the "extinction direction net" for the uniaxial flash figure—it rather resembles a stereographic projection of the reference sphere—and Fig. 19*b* represents the net for an optic normal figure of $2V = 90°$.

Acknowledgments

I wish to thank Prof. George Tunell and Prof. A. E. J. Engel for helpful advice and discussion. I am grateful to Prof. Horace Winchell for valuable suggestions and criticism of the manuscript.

References

Becke, F. (1904), *Denk. Akad. Wiss. Wien, Math.-Naturw. Klasse*, **75**.
——— (1905), *Tsch. Min. Pet. Mitt.*, **24,** 1–34.
——— (1909), *Tsch. Min. Pet. Mitt.*, **28,** 290–293.
Burri, C. (1950), *Das Polarisationsmikroskop:* Basel.
Evans, J. W. (1907), *Min. Mag.*, **14,** 276–280.
Johannsen, A. (1918), *Manual of Petrographic Methods:* N. Y.
Kaemmerer (1913), *Fort. d. Min.*, **3,** 141–158.
Michel-Lévy, A. (1888), *Les Minéraux d. Roches*, 94–95.
Souza-Brandao (1914), *Z. Krist.*, **54,** 113–119.
Tröger, W. E. (1956), *Optische Bestimmung der gesteinsbildenden Minerale:* Stuttgart.
Wahlstrom, E. E. (1951), *Optical Crystallography:* N. Y.
Winchell, A. N. and Winchell, H. (1951), *Optical Mineralogy*, Part II: N. Y.
Wright, F. E. (1905), *Am. J. Sci.* (4), **20,** 285.
——— (1907), *Am. J. Sci.* (4), **24,** 317.
——— (1911a), *Am. J. Sci.* (4), **31,** 157–211.
——— (1911b), *Carnegie Inst. Wash. Pub.*, **158,** 75–76.
——— (1923), *J. Opt. Soc. Amer.*, **7,** 779–817.